Development and validation of a computed tomography-based immune ecosystem diversity index as an imaging biomarker in non-small cell lung cancer

European Radiology (2022) 32:8726–8736
https://doi.org/10.1007/s00330-022-08873-6

IMAGING INFORMATICS AND ARTIFICIAL INTELLIGENCE

Development and validation of a computed tomography–based immune ecosystem diversity index as an imaging biomarker in non-small cell lung cancer

Lan He[1] · Zhen-Hui Li[1,2] · Li-Xu Yan[3] · Xin Chen[4] · Sebastian Sanduleanu[5] · Wen-Zhao Zhong[6] · Phillippe Lambin[5,7] · Zhao-Xiang Ye[8] · Ying-Shi Sun[9] · Yu-Lin Liu[10] · Jin-Rong Qu[11] · Lin Wu[12] · Chang-Ling Tu[13] · Madeleine Scrivener[14] · Thierry Pieters[15] · Emmanuel Coche[16] · Qian Yang[10] · Mei Yang[17] · Chang-Hong Liang[1,19] · Yan-Qi Huang[1,18] · Zai-Yi Liu[1,19]

Received: 28 September 2021 / Revised: 22 April 2022 / Accepted: 11 May 2022 / Published online: 31 May 2022

Abstract

Objectives To date, there are no data on the noninvasive surrogate of intratumoural immune status that could be prognostic of survival outcomes in non-small cell lung cancer (NSCLC). We aimed to develop and validate the immune ecosystem diversity index (iEDI), an imaging biomarker, to indicate the intratumoural immune status in NSCLC. We further investigated the clinical relevance of the biomarker for survival prediction.

Methods In this retrospective study, two independent NSCLC cohorts (Resec1, n = 149; Resec2, n = 97) were included to develop and validate the iEDI to classify the intratumoural immune status. Paraffin-embedded resected specimens in Resec1 and Resec2 were stained by immunohistochemistry, and the density percentiles of $CD3^+$, $CD4^+$, and $CD8^+$ T cells to all cells were quantified to estimate intratumoural immune status. Then, EDI features were extracted using preoperative computed tomography to develop an imaging biomarker, called iEDI, to determine the immune status. The prognostic value of iEDI was investigated on NSCLC patients receiving surgical resection (Resec1; Resec2; internal cohort Resec3, n = 419; external cohort Resec4, n = 96; and TCIA cohort Resec5, n = 55).

Results iEDI successfully classified immune status in Resec1 (AUC 0.771, 95% confidence interval [CI] 0.759–0.783; and 0.770 through internal validation) and Resec2 (0.669, 0.647–0.691). Patients with higher iEDI-score had longer overall survival (OS) in Resec3 (unadjusted hazard ratio 0.335, 95%CI 0.206–0.546, $p < 0.001$), Resec4 (0.199, 0.040–1.000, $p < 0.001$), and TCIA (0.303, 0.098–0.944, $p = 0.001$).

Conclusions iEDI is a non-invasive surrogate of intratumoural immune status and prognostic of OS for NSCLC patients receiving surgical resection.

Key Points

- *Decoding tumour immune microenvironment enables advanced biomarkers identification.*
- *Immune ecosystem diversity index characterises intratumoural immune status noninvasively.*
- *Immune ecosystem diversity index is prognostic for NSCLC patients.*

Keywords Non-small cell lung cancer · Immunohistochemistry · Ecosystem · Prognosis · Computed tomography

Lan He and Zhen-Hui Li contributed equally as co-first authors.

Yan-Qi Huang and Zai-Yi Liu contributed equally as co-senior authors.

✉ Yan-Qi Huang
yikiann@126.com

✉ Zai-Yi Liu
zyliu@163.com

Extended author information available on the last page of the article

Abbreviations

AJCC	American Joint Committee Cancer
AUC	Area under the ROC curve
CI	Confidence interval
iAUC	Integrated area under the ROC curve
iBS	Integrated Brier score
iEDI	Immune ecosystem diversity index
LASSO	The least absolute shrinkage and selection operator
NCCN	National Comprehensive Cancer Network

NNE	Nearest Neighbor Estimation
NSCLC	Non-small cell lung cancer
OS	Overall survival
ROC	Receiver operating characteristic
TIME	Tumour immune microenvironment
TNM	Tumour-node-metastasis

Introduction

Non-small cell lung cancer (NSCLC) accounts for approximately 85% of lung cancer [1]. Although the American Joint Committee Cancer (AJCC) tumour-node-metastasis (TNM) staging system provides reliable information regarding routine prognostication and treatment decision [2], there remains considerable room for improvement, as distinct clinical outcomes are observed among patients with NSCLC of the same TNM stage [3, 4]. These facts highlight the unmet clinical requirement for robust biomarkers to improve patient stratification.

Accumulating evidence demonstrates that cancer evolution is strongly dependent on the complex tumour immune microenvironment (TIME) in which it develops [5–7]. As one of the notable constituents of the TIME, the prognostic role of tumour-infiltrating immune cells has been thoroughly investigated in various neoplasms, and emerging data have confirmed its superiority to the classical TNM staging system [8–10]. For example, the densities and location of specific T cell infiltrations, such as those of $CD3^+$, $CD4^+$, and $CD8^+$ T cells, were associated with the prognosis of lung cancer [3, 9, 11–14]. This supports the hypothesis that characterisation of the intratumoural immune status within the TIME may be a feasible approach for identifying advanced biomarkers [4].

In clinical practice, a non-invasive approach to assess the intratumoural immune status in NSCLC is still required [15–18]. Fortunately, a recent pioneering work has provided a foundation for future studies focussing on the non-invasive radiomics approach to infer immune phenotype and predict outcomes [11]. However, a concern was raised by Sun et al to account for image acquisition variability in radiomics study, which calls for methodological refinement for broad application. Therefore, the aim of this study was to utilise a new radiomics approach to characterise the intratumoural immune status without requiring imaging pre-processing to ensure enough robustness and generalisation, through the development of an immune ecosystem diversity index (iEDI) to decode the spatial heterogeneity within the tumour. Sub-region EDI features were extracted in our approach, instead of extracting simple 'average value' measurements within the tumour. We further investigated its prognostic value for overall survival (OS) prediction for NSCLC patients who underwent surgical resection.

Materials and methods

Study design and clinical cohorts

Ethical approval was obtained for this retrospective study, and the informed consent requirement was waived. In this international and multi-cohort study, five independent cohorts of NSCLC patients were included (Fig. 1). The Resec1 training cohort consisted of 149 resected NSCLC patients. Both preoperative CT images and paraffin-embedded sections of the resected tumour specimens were acquired. This cohort was used to develop iEDI and characterise intratumoural immune status. The Resec2 validation cohort consisted of 97 resected NSCLC patients, with preoperative CT and paraffin-embedded sections of resected tumour specimens acquired. This cohort was used to validate the association of iEDI with intratumoural immune status. And the internal validation was performed by using 1000 bootstrap resamples of Resec1 cohort.

The remaining 3 cohorts were used to investigate the clinical relevance of iEDI for survival prediction in patients treated with resection. Cohort Resec3 (n = 419), Resec4 (n = 96), and Cancer Imaging Archive (TCIA, n = 55) [19, 20] consisted of patients who had undergone resection, on which the prediction performance of iEDI for OS was evaluated.

All patients were treated according to the National Comprehensive Cancer Network (NCCN) [21]. Baseline pretreatment contrast-enhanced CT images and clinical data were acquired. The details of inclusion and exclusion criteria, clinical outcomes of interest, and the follow-up procedure were described in Supplementary Methods (p2-p3 in the Supplement). The details of parameters of CT image scanning for all cohorts were described in Supplementary Methods (p3 in the Supplement).

Procedure

Estimation of intratumoural immune status

IHC staining was performed for tumour tissues in Resec1 and Resec2 cohorts. The procedure of T cells staining and counting was described in Supplementary Methods (p4 in the Supplement).

To decode tumour cell-lymphocyte interaction in TIME [7], the ratio of lymphocytes ($CD3^+$, $CD4^+$, and $CD8^+$T cells) to all cells in two regions (tumoural centre [TC] and invasive margin [IM], Supplementary Fig. 1) was considered the immune features. Regions of tumoural centre and invasive margin were defined by a board-certified lung cancer pathologist who also performed the cell counting. Thereby, six immune features were obtained for each patient ($CD3^+$TC, $CD3^+$IM, $CD4^+$TC, $CD4^+$IM, $CD8^+$TC, and $CD8^+$IM). After that, the least absolute shrinkage and selection operator (LASSO) Cox

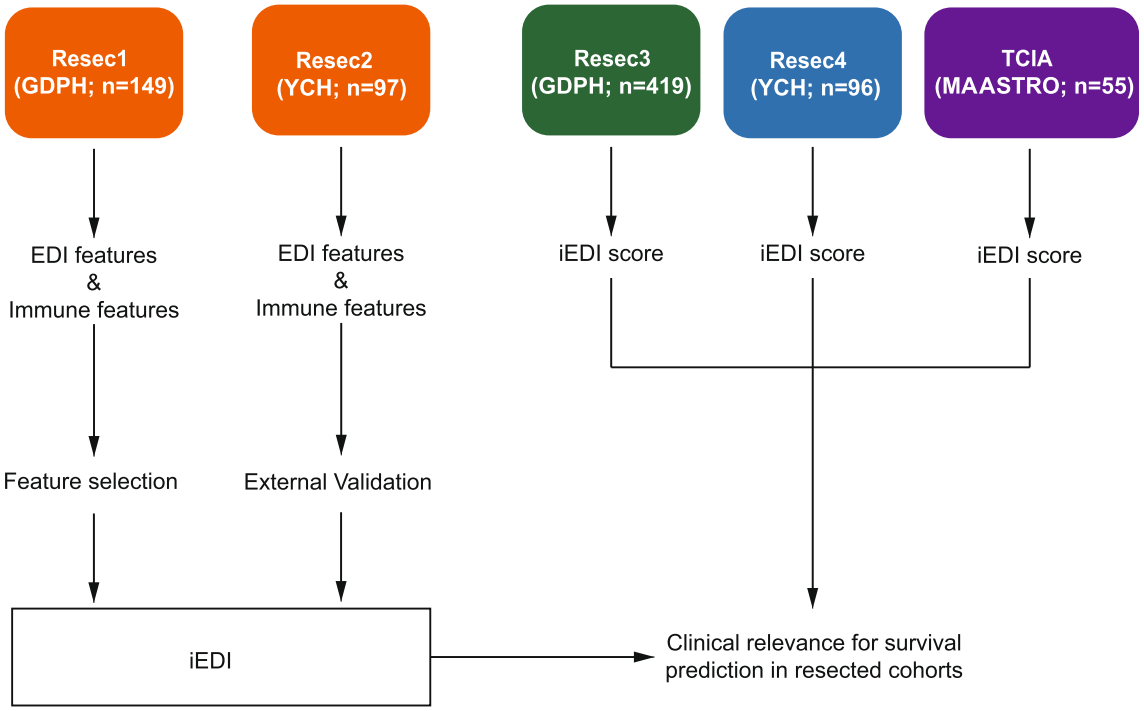

Fig. 1 Study design flowchart. EDI, ecosystem diversity index; iEDI, immune ecosystem diversity index; GDPH, Guangdong Provincial People's Hospital; YCH, Yunnan Cancer Hospital; MAASTRO, MAASTRO Clinic

regression analysis with 10-fold cross-validation was performed on the Resec1 cohort for immune feature selection, with which an immune signature was developed. The target value for this LASSO Cox regression analysis was OS time. The immune score was computed per patient according to the immune signature, using a linear combination of selected immune features weighted by their respective coefficients. Then, the patients were classified into distinct intratumoural immune status (high-level *vs.* low-level) according to the immune score, with the optimal threshold identified by the time-dependent receiver operating characteristic (ROC) analyses using the Nearest Neighbor Estimation (NNE) method [22].

Extraction of ecosystem diversity index feature

The in-house Matlab-based extraction algorithm was applied to all cohorts, with the images of all cohorts being centralised. Based on the concept of EDI proposed by Natrajan et al [6], we utilised volumetric EDI feature extraction on pretreatment contrast-enhanced CT images to describe TIME (Fig. 2). First, the tumour contour was delineated on preoperative contrast-enhanced CT images; then, the tumour region was divided into multiple non-overlapping sub-regions of m by m pixels. (To identify regional clusters within a tumour, tumour regions needed to be small enough so that there were sufficient numbers of regions, yet sufficiently large to measure intratumoural heterogeneity of TIME. In this study, we explored the range of 3 to 10 for the value of m. We used at least 3 as the value of m, because of the minimum unit area to ensure the correct calculation of features. And the maximum of 10 as the value of m was used to avoid small subregions groups. The numbers of sub-regions divided within a single tumour are shown in Supplementary Table 1. Based on the results described in Supplementary Fig. 2 and Supplementary Table 3, the optimization of the region size was 5*5 in our study.) If there were multiple disconnected tumour volumes, the largest tumour volume was used for feature extraction.

A total of 45 radiomics features were extracted from each sub-region (feature extraction algorithm and optimisation of sub-region size were provided in Supplementary Methods [p4-p6 in the Supplement], Supplementary Table 2 and Supplementary Table 3). Therefore, each sub-region would have 45 radiomics features for clustering. Then for each radiomics feature, the Gaussian mixture model unsupervised clustering was used to identify the optimal number (K) of clusters of sub-regional values within tumour volume in an unbiased manner [23]. K, ranging from 1 to 5, could describe the distribution of each feature and reflect the degree of spatial heterogeneity in the entire tumour volume and was termed the 'EDI feature'. Through this process, each patient would have obtained 45 EDI features. The details of the Gaussian mixture model unsupervised clustering algorithm were provided in Supplementary Methods p6.

The intra- and inter-observer agreement of the EDI features extraction were provided in Supplementary Methods (p6-p7 in the Supplement).

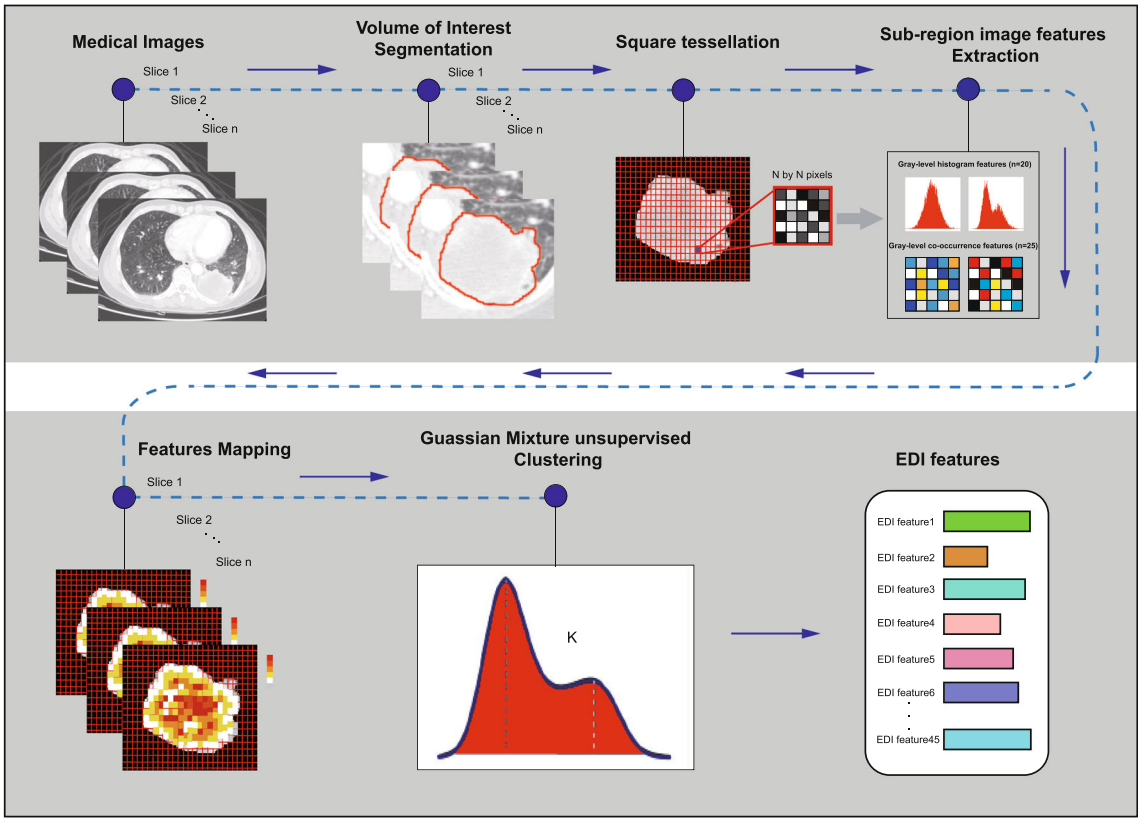

Fig. 2 The workflow showing EDI feature extraction. Image segmentation is performed on contrast-enhanced computed tomography (CT) images. Volume of interest (VOI) is delineated initially around the tumour outline by experienced radiologists. The tumour volume region is divided into multiple non-overlapping sub-regions of *m* by *m* pixels; Then, 45 radiomics features are extracted from each sub-region. Thus, each sub-region will have 45 radiomics features for clustering. Afterwards, the Gaussian mixture model unsupervised clustering is used to identify the optimal number (K) of clusters of sub-regional values of each radiomics feature within tumour volume in an unbiased manner. The optimal K value is describing the distribution for each radiomics feature within tumour volume, which is termed the 'EDI feature' in our study. Through this process, each patient will have obtained 45 EDI features, which are reflecting the degree of spatial heterogeneity in the entire tumour volume.

iEDI development

To develop an immune-informed imaging biomarker called iEDI, the LASSO logistic regression analysis with 10-fold cross-validation was performed to select the most relevant EDI features related to the estimated intratumoural immune status (high level *vs.* low level) in cohort Resec1. The target value for this LASSO logistic regression analysis was immune status. A score of iEDI (iEDI-score) was computed per patient using a linear combination of selected EDI features weighted by their respective coefficients.

iEDI assessment and validation

The potential association of iEDI with the intratumoural immune status was first assessed in cohort Resec1 and then validated in an independent cohort, Resec2, using the Mann-Whitney *U* test. The iEDI was also subjected to 1000 bootstrap resamples for internal validation of the Resec1 cohort.

Prognostic value of iEDI for survival prediction on resected cohorts

We further investigated the prognostic value of iEDI for OS prediction in patients receiving surgical resection. Kaplan-Meier analyses were performed on patient groups (high iEDI-score vs. low iEDI-score), with an optimal cut-off of the iEDI-score identified by the time-dependent ROC analysis using the NNE method. Univariate association between iEDI and OS was evaluated using the log-rank test and Cox proportional hazards model. A multivariate Cox model was used to assess the associations between iEDI and OS after adjusting for potential confounders including sex, age, smoking history, histological type, AJCC/Union for International Cancer Control (UICC) TNM stage, and tumour volume. Stratified multivariable Cox model analysis was performed, where the centre was used as the stratification factor. Prediction performance was assessed with respect to the area under the ROC curve (AUC), the integrated area under the ROC curve (iAUC), and the integrated Brier score (iBS). The iBS is an

integrated measurement of the mean squared error over time, which ranges from 0 for a perfect predictor to 0.25 for a non-informative predictor with a 50% incidence of the outcome.

Statistical analysis was conducted using the R software (version 4.1.3, https://www.r-project.org). R packages were described in Supplementary Methods (p7 in the Supplement). The Mann-Whitney *U* test, Kruskal-Wallis test, and chi-square test were used wherever applicable.

Results

Patients

Table 1 summarised the basic patient demographics and clinical characteristics for all cohorts. Data from the international cohort, the TCIA, which consisted of patients treated at the MAASTRO Clinic, The Netherlands, was retrieved from the databases of TCIA [19, 20]. The median OS time was 43.0 (interquartile range (IQR): 21.0–71.5) months in the Resec1 cohort, 46.6 (IQR: 23.8–57.8) months in the Resec2 cohort, 43.0 (IQR: 28.0–60.0) months in Resec3 cohort, 58.9 (IQR: 54.5–66.9) months in Resec4 cohort, and 39.0 (IQR: 20.4–70.2) months in TCIA cohort, respectively. The median follow-up time was 53.6 (IQR: 24.9–73.1) months in the Resec1 cohort, 45.4 (IQR: 22.8–60.5) months in the Resec2 cohort, 49.1 (IQR: 34.7–63.8) months in Resec3 cohort, 58.8 (IQR: 47.2–66.8) months in Resec4 cohort, and 39.0 (IQR: 20.4–70.2) months in TCIA cohort, respectively (Table 1).

Immune status estimation and assessment

No significant differences were observed in the immune features between Resec1 and Resec2 (p = .05–.927; Supplementary Table 4). The immune signature was constructed with four immune features, namely the percentile of $CD3^{+}_{TC}$, $CD4^{+}_{IM}$, $CD8^{+}_{TC}$, and $CD8^{+}_{IM}$ to all cells. (The immune score calculation formula was shown in Supplementary Methods [p7 in the Supplement].) There was no statistical difference in median immune scores between Resec1 (−0.410 [interquartile range, IQR: -0.808, -0.126]) and Resec2 (-0.390 [-0.710, 0.088]), (p = .330). The binary immune status was determined by the derived immune scores (high-level [immune-score ≥ -0.317] *vs.* low-level [< −0.317], Supplementary Fig. 3). Patients with higher baseline immune score showed improved OS, in both Resec1 (hazard ratio [HR] 0.190 [95% CI 0.091–0.398], p <0.001) and Resec2 (0.262, [0.127–0.539], p <0.001) (Supplementary Fig. 4). For OS prediction, the immune signature provided an AUC of 0.755 (95% confidence interval [CI]: 0.742–0.768) in Resec1, 0.754 through the internal validation, and 0.712 (0.696–0.728) in Resec2.

iEDI construction, evaluation, and validation

The resulting iEDI consisted of 10 EDI features (Supplementary Fig. 5), and individual iEDI scores were calculated for every patient using the formula in Supplementary Methods (p6-p7 in the Supplement). Significant difference was observed in the iEDI scores between patient groups defined by immune status, in both cohort Resec1 (p < .001) and Resec2 (p = .004), wherein iEDI scores were higher for patients with high-level immune status (high-level *vs.* low-level: 0.70 ± 0.619 *vs.* -0.04 ± 0.642 in Resec1, 0.875 ± 0.518 *vs.* -0.055 ± 0.614 in Resec2; Supplementary Fig. 6). For immune status discrimination, the iEDI yielded an AUC of 0.771 (95% CI: 0.759–0.783) in Resec1, 0.770 through the internal validation, and 0.669 (0.647–0.691) in Resec2.

Prognostic value of iEDI for survival prediction on resected cohorts

Higher baseline iEDI score was associated with improved OS (cut-off value: -0.291; Resec1 [unadjusted HR 0.112, 95% CI 0.053–0.239, p <0.001], Resec2 [0.271, 0.096–0.763, p <0.001], Resec3 [0.335, 0.206–0.546, p <0.001], Resec4 [0.199, 0.040–1.000, p <0.001], TCIA [0.303, 0.098–0.944, p = 0.001], Fig. 3). The OS and survival rate in the high iEDI-score and low iEDI-score group for all cohorts were listed in Table 2. For the discrimination of OS prediction, iEDI provided an AUC of 0.790 (95% CI 0.780–0.800) in Resec1, 0.789 through the internal validation, 0.701 (0.684–0.718) in Resec2, 0.692 (0.687–0.697) in Resec3, 0.705 (0.678–0.732) in Resec4, and 0.745 (0.721–0.769) in TCIA. The iAUC was 0.755 in Resec1, 0.684 in Resec2, 0.655 in Resec3, 0.707 in Resec4, and 0.687 in TCIA. And the iBS was 0.138 in Resec1, 0.146 in Resec2, 0.142 in Resec3, 0.087 in Resec4, and 0.170 in TCIA. Multivariate analysis showed that iEDI remained a significant predictor of OS even after adjusting for clinicopathological confounders (Table 3, all p <0.05). The results of stratified multivariable Cox regression analysis showed that iEDI was a predictor independent of tumour volume and TNM staging (Supplementary Table 5 and Supplementary Table 6, all p <0.05).

Discussion

In this study, we utilised sub-region radiomics analysis of pretreatment CT to develop a non-invasive biomarker for NSCLC, called iEDI. With clear biological interpretability related to intratumoural immune status, the proposed iEDI was shown to be an independent prognostic factor for OS on independent cohorts of patients with NSCLC who underwent surgical resection.

Table 1 Baseline characteristics and clinical characteristics of resected NSCLC cohorts

Characteristics	Resec1 (GDPH; 149)	Resec2 (YCH; 97)	Resec3 (GDPH; 419)	Resec4 (YCH; 96)	TCIA (MAASTRO; 55)	*p*
Age (y, median[IQR])	61 (55, 68)	56 (48, 63)	61 (54, 68)	56 (49, 64)	NA	< 0.001
Sex						
Male	86 (57.7%)	60 (61.9%)	273 (65.2%)	61 (63.5%)	36 (65.5%)	0.245
Female	63 (42.3%)	37 (38.1%)	146 (34.8%)	35 (36.5%)	19 (34.5%)	
Smoking status						
Yes	40 (26.8%)	43 (44.3%)	153 (36.5%)	43 (44.8%)	NA	0.01
No	109 (73.2%)	54 (55.7%)	266 (63.5%)	53 (55.2%)		
Histological type						
Adenocarcinoma	109 (73.2%)	69 (71.1%)	319 (76.1%)	78 (81.3%)	29 (52.7%)	
Others	40 (26.8%)	28 (28.9%)	100 (23.9%)	18 (18.8%)	26 (47.3%)	
T stage						
T1	57 (38.3%)	58 (59.8%)	170 (40.6%)	71 (74.0%)	NA	< 0.001
T2	72 (48.3%)	31 (32.0%)	204 (48.7%)	20 (20.8%)		
T3	19 (12.8%)	4 (4.1%)	38 (9.1%)	3 (3.1%)		
T4	1 (0.7%)	4 (4.1%)	7 (1.7%)	2 (2.1%)		
N stage						
N0	113 (75.8%)	58 (59.8%)	318 (75.9%)	78 (81.3%)	NA	0.007
N1	12 (8.1%)	19 (19.6%)	34 (8.1%)	8 (8.3%)		
N2	24 (16.1%)	20 (20.6%)	67 (16.0%)	10 (10.4%)		
N3	0	0	0	0		
Follow-up time (mo)						
Median	53.6	45.4	49.1	58.8	39.0	< 0.001
IQR	(24.9, 73.1)	(22.8, 60.5)	(34.7, 63.8)	(47.2, 66.8)	(20.4, 70.2)	
iEDI score						
Median	−0.564	−0.784	−0.648	−0.821	−0.653	< 0.001
IQR	(−0.904, 0.013)	(−1.116,− 0.343)	(−0.999, −0.098)	(−1.139, −0.442)	(−1.072, −0.327)	

Note: *NA*, not available; *y*, years; *mo*, month; *iEDI*, image-based ecosystem diversity index; *IQR*, interquartile range. *GDPH*, Guangdong Provincial People's Hospital; *YCH*, Yunnan Cancer Hospital; *MAASTRO*, MAASTRO Clinic

Despite strong clinical indications, the immune-informed biomarker has to be reliable and standardised to ensure its generalised usage across various sources of technical variability. In particular, methodological refinement for broad application is warranted to account for image acquisition variability in retrospective radiomics studies [24]. Therefore, sub-region analysis of the tumour volume was adopted in our radiomics approach, instead of extracting simple 'average value' measurements within tumour. Sub-regional EDI features were generated in our approach to quantify the degree of spatial heterogeneity. The concept of 'EDI' was put forward by Natrajan et al, who applied it to cancer research to decode the spatial heterogeneity within the tumour microenvironment based on histological sample analysis [6, 25], while its origin can be traced back to the diversification of tumour ecosystem [26–28]. To the best of our knowledge, this is the first study to utilise EDI analysis in radiomics study. The final clustered value of K was determined as a EDI feature, to describe the distribution of each feature within tumour volume so as to characterise the heterogeneity of each feature across the tumour volume. Our strategy has a dual advantage: first, the extracted features are small-scale, which will reduce overfitting; second, the input EDI features can be considered standardised features. This will reduce variability to ensure broad application.

As a benchmark for the utility of our EDI features, we also extracted volume-averaged radiomics features; results showed that the iEDI demonstrated better discrimination performance for survival prediction across all datasets than the immune-informed radiomics signature (Supplementary Methods [p7-p8 in the Supplement]; Supplementary Table 7). This suggests that EDI features are not sensitive to image acquisition variability across cohorts, and have superior prediction ability compared to that of the current practice of radiomics analysis. As such, this reproducible method that does not require any imaging pre-processing can be used to reach the full potential

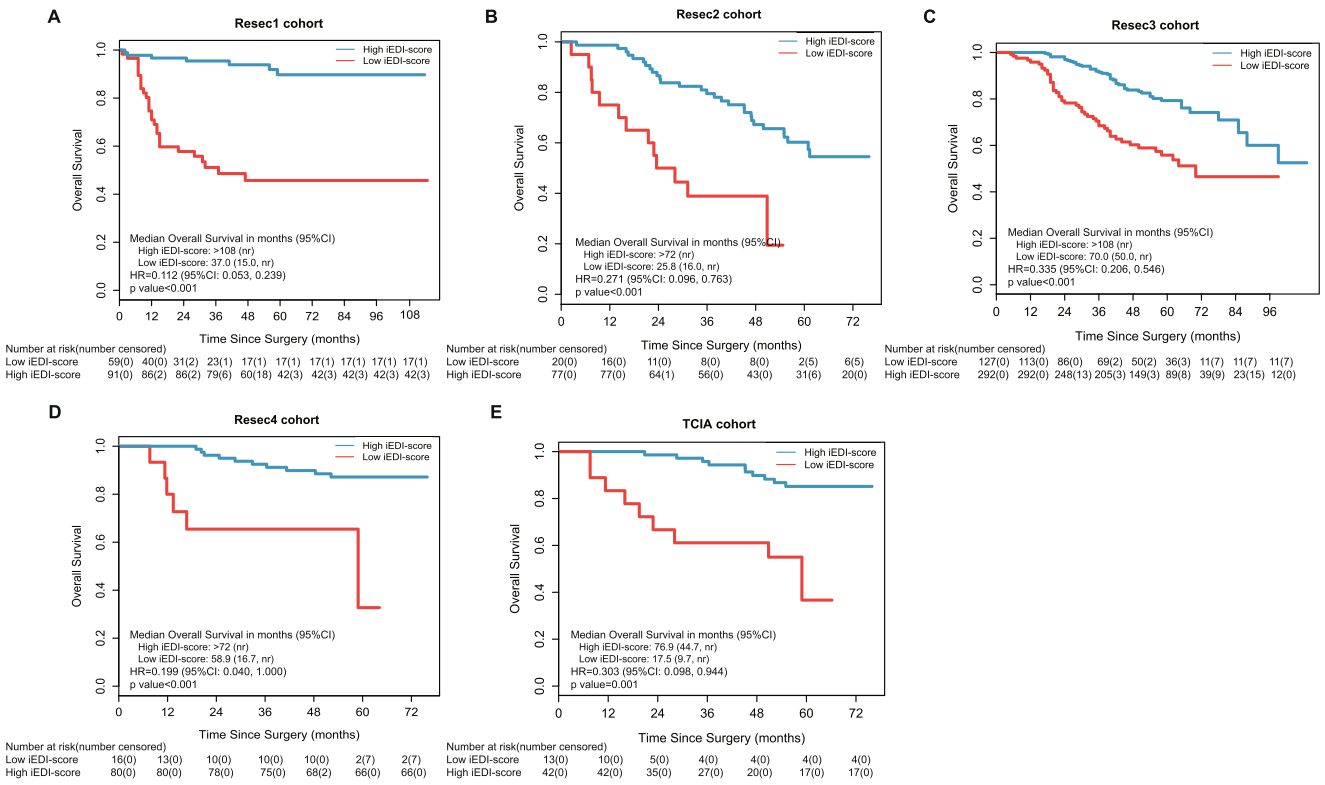

Fig. 3 Kaplan-Meier curves for overall survival (OS) according to iEDI score. Cohort Resec1 (**A**), Resec2 (**B**), Resec3 (**C**), Resec4 (**D**), and TCIA (**E**). Patients were stratified into high iEDI-score or low iEDI-score group according to individual iEDI-score based on the cut-off value (-0.291) identified in Resec1. nr, not reached at maximal follow-up time

of radiomics and address the challenges regarding the harmonisation and standardisation of image acquisition protocols associated with retrospective or multi-centre studies [29].

Using this innovative approach, we continued the recent ongoing research effort of making radiomics more interpretable, by presenting iEDI as a surrogate of intratumoural immune status [7, 11, 30, 31]. Motivated by the recent pioneering work of Sun et al, our study did not focus only on revealing the biological basis of the radiomic biomarker regarding immune infiltration, but also provided a step forward outcomes prediction [11]. Notably, this study is one of the few investigations utilising an immune-informed approach to establish a link between underlying pathology and clinical outcomes [11, 19, 30, 32]. For resectable NSCLC, iEDI successfully achieved patient stratification with respect to OS on five cohorts and remained an independent predictor adjusted for clinicopathological parameters (including T and N staging, and tumour volume). This observation was consistent with previous studies on NSCLC, indicating the strong potential of the immune-informed biomarker to stratify risk beyond staging [3, 4, 9, 33]. In addition, iEDI showed superior prediction performance compared with TNM stage and tumour volume (Supplementary Methods [p8-p9 in the Supplement]; Fig. 4; Supplementary Table 8). Furthermore, iEDI provided incremental predictive value when incorporated into a prediction model integrating all independent risk factors, including the TNM stage (Supplementary Table 8). Altogether, our observations demonstrated the potential of iEDI to translate our evolving understanding of TIME into better patient stratification beyond TNM staging.

Despite the widespread interest in various malignancies regarding the characterisation of TIME, such studies on NSCLC are sparse, with no general recommendations on immune cell markers [4, 9, 17], whereas studies on colorectal cancer and breast cancer are about to achieve that goal [4, 34–37]. Particularly in colorectal cancer, multinational efforts had demonstrated that immunoscore, which is derived based on the density of CD3+ and CD8+ T cells in both tumor centre and invasive margins, had been proposed as a standardised, reliable measurement of immune prognostic markers [34–37]. Serial studies had demonstrated that $CD3^+$, $CD4^+$, $CD45RO^+$, and $CD8^+$ T cells had prognostic value in NSCLC [3, 4, 9]. With regard to the CD45RO cells, recent studies revealed that their prognostic values remained uncertain. Hence, the immune cell markers of interest in our study included $CD3^+$, $CD4^+$, and $CD8^+$ T cells in both TC and IM regions. Considering the intricate interaction between cancer cells and lymphocytes [34], we also had validated whether the immune biomarker by using the ratios (percentile) of lymphocytes to all cells was showing better prognostic value for OS predicting compared with the immune biomarker based on the number of immune cells. The results showed that the immune

Table 2 OS and survival rate in the high iEDI-score and low iEDI-score group for all cohort

Parameter	Resec1			Resec2			Resec3			Resec4			TCIA		
	High iEDI-score	Low iEDI-score	Total	High iEDI-score	Low iEDI-score	Total	High iEDI-score	Low iEDI-score	Total	High iEDI-score	Low iEDI-score	Total	High iEDI-score	Low iEDI-score	Total
No. of patients [n (%)]	91 (53.8)	58 (34.2)	149	77 (79.4)	20 (20.6)	97	292 (69.7)	127 (30.7)	419	80 (83.3)	16 (16.7)	96	42 (76.4)	13 (23.6)	55
3-years OS [median (IQR)] (month)	56.0 (35.0, 85.0)	25.0 (9.8, 53.0)	43.0 (21.0, 71.5)	55.0 (31.7, 61.4)	23.8 (10.6, 39.2)	46.6 (23.8, 57.8)	46.0 (33.0, 61.0)	37.0 (20.0, 59.0)	43.0 (28.0, 60.0)	61.4 (55.0, 67.6)	49.5 (12.1, 57.9)	58.9 (54.5, 66.9)	42.2 (24.4, 73.0)	17.5 (8.5, 43.2)	39.0 (20.4, 70.2)
No. of survival [n (%)]															
At 3 years	84 (92.3)	30 (51.7)	114 (76.5)	48 (62.3)	7 (35.0)	55 (56.7)	243 (83.2)	79 (62.2)	322 (76.8)	70 (87.5)	10 (62.5)	80 (83.3)	21 (50.0)	3 (23.1)	24 (43.6)
At 1 year	85 (93.4)	32 (55.2)	117 (78.5)	76 (98.7)	15 (25.0)	91 (93.8)	261 (89.4)	94 (74.0)	355 (84.7)	80 (100)	13 (81.3)	93 (96.9)	41 (97.6)	9 (69.2)	50 (90.9)

Note. *OS*, overall survival; *IQR*, interquartile range

Table 3 The multivariate analysis for assessing the associations between iEDI and OS after adjusting for potential confounders

Variables/C-index	Resec1 cohort			Resec2 cohort			Resec3 cohort			Resec4 cohort			TCIA cohort*		
	Coefficient	HR (95% CI)	*p*	Coefficient	HR (95% CI)	P	Coefficient	HR (95% CI)	P	Coefficient	HR (95% CI)	P	Coefficient	HR (95% CI)	*p*
Histology	−1.018	0.361 (0.195, 0.670)	0.001	-	-	-	-	-	-	-	-	-	—	-	-
T stage	1.054	2.869 (1.601, 5.139)	0.0004	-	-	-	-	-	-	-	-	-	-	-	-
N stage	0.558	1.747 (1.206, 2.532)	0.003	-	-	-	0.794	2.213 (1.781, 2.750)	< .001	0.759	2.135 (1.158, 3.938)	.015	-	-	-
Clinical stage	-	-	-	0.958	2.607 (1.721, 3.948)	<0.001	-	-	-	-	-	-	-	-	-
iEDI	−1.775	0.170 (0.068, 0.426)	0.002	−0.895	0.408 (0.200, 0.835)	0.014	−0.801	0.449 (0.299, 0.674)	.001	−1.853	0.157 (0.053, 0.464)	.001	−1.194	0.303 (0.098, 0.944)	.001
C-index (95%CI)	0.864 (0.855, 0.873)			0.745 (0.729, 0.761)			0.750 (0.745, 0.755)			0.656 (0.627, 0.685)			0.745 (0.721, 0.769)		

Note. *iEDI*, image-based ecosystem diversity index; *HR*, hazard ratio; *95% CI*, 95% confidence interval; *NA*, not available. *The variables of T stage and N stage for TCIA cohort were unavailable

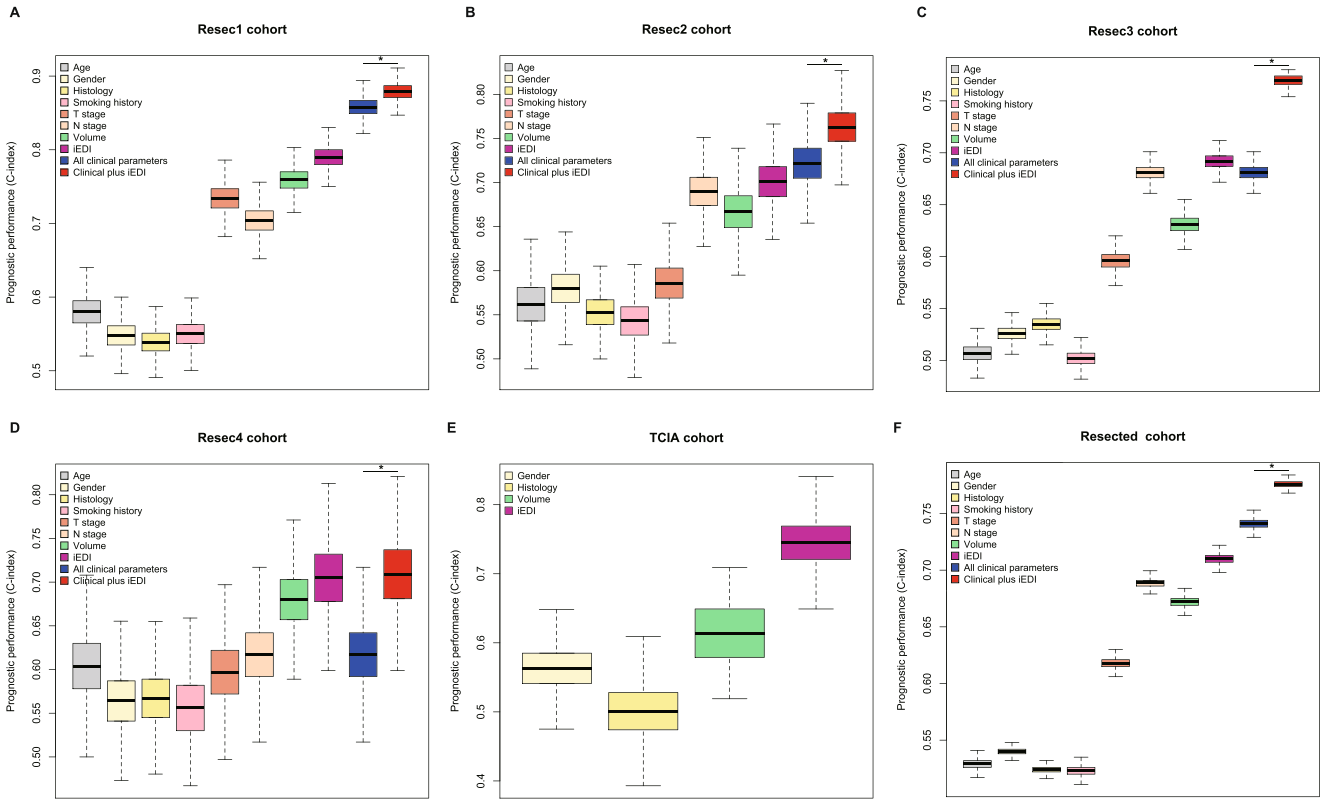

Fig. 4 Clinical performance of iEDI, tumour volume, and tumour-related risk parameters. Cohort Resec1 (**A**), Resec2 (**B**), Resec3 (**C**), Resec4 (**D**), TCIA (**E**), and Resected cohort (combined of Resec1 to Resec4 cohorts, **F**)

biomarker based on the number of immune cells has lower values than the immune biomarker constructed using the ratios (percentile) of lymphocytes to all cells for classifying high-risk *vs.* low-risk patient groups based on OS (Supplementary Table 9 and Supplementary Table 10). Thus, we constructed and validated the immune signature using the percentiles of lymphocytes in all cells.

Our study has some limitations. First, the analyses were based on retrospective data collection. Second, no consensus had been reached regarding a consent framework on the quantification of immune infiltration in NSCLC, with few comparable results available; hence, we believed that the task force dedicated to establishing a well-standardised paradigm should be initiated in the near future. This would subsequently underscore the necessity of further readjusting the iEDI for clinical practice. Lastly, though iEDI was valid for prediction across various treatment regimens, the best cut-offs were established regarding each individual therapy, and were different as expected, since the pretreatment baseline condition of the patients receiving various therapies was distinct and the biomarker was derived based on pretreatment images. Additionally, the corresponding best cut-off had been validated using independent cohorts.

In conclusion, we established and validated a biomarker based on pretreatment CT, called iEDI, to interpret the intratumoural immune status of TIME in NSCLC. Our findings showed that this novel biomarker might be an efficient, non-invasive, and reliable tool for clinical outcome prediction, which will potentially assist in personalised treatment regimen selection for patients with NSCLC. Our work had expanded the frontiers of radiomics into the area, revealing causality to clinical outcomes by inferring both the biological basis of immune infiltration and clinical relevance regarding survival outcomes.

Supplementary Information The online version contains supplementary material available at https://doi.org/10.1007/s00330-022-08873-6.

Acknowledgements We thank The Cancer Imaging Archive.

Funding This study was supported by the National Key Research and Development Program of China (grant number 2021YFF1201003), the Key R&D Program of Guangdong Province of China (grant number 2021B0101420006), the National Science Fund for Distinguished Young Scholars (grant number 81925023), and the National Natural Scientific Foundation of China (grant number 81771912, 81901910, 82071892, and 82001986), the High-level Hospital Construction Project (DFJHBF202105). The funding sources had no involvement in study design, in the collection, analysis, and interpretation of data, in the writing of the report, and in the decision to submit the article for publication.

Declarations

Guarantor The scientific guarantor of this publication is Zaiyi Liu.

Conflict of interest The authors of this manuscript declare no relationships with any companies, whose products or services may be related to the subject matter of the article.

Statistics and biometry One of the authors has significant statistical expertise.

Informed consent Written informed consent was waived by the Institutional Review Board.

Ethical approval Institutional Review Board approval was obtained.

Methodology
- retrospective
- prognostic study
- multicentre study

References

1. Siegel RL, Miller KD, Jemal A (2018) Cancer statistics. CA Cancer J Clin 68(1):7–30
2. Edge S, Byrd D, Compton C, Fritz A, Greene F, Trotti A (2010) AJCC cancer staging manual, 7th edn. Springer, Berlin Heidelberg New York
3. Donnem T, Hald SM, Paulsen EE et al (2015) Stromal CD8+ T-cell density-a promising supplement to TNM staging in non-small cell lung cancer. Clin Cancer Res 21(11):2635–2643
4. Donnem T, Kilvaer TK, Andersen S et al (2016) Strategies for clinical implementation of TNM-Immunoscore in resected nonsmall-cell lung cancer. Ann Oncol 27(2):225–232
5. Junttila MR, de Sauvage FJ (2013) Influence of tumour microenvironment heterogeneity on therapeutic response. Nature 501(7467):346–354
6. Natrajan R, Sailem H, Mardakheh FK et al (2016) Microenvironmental heterogeneity parallels breast cancer progression: a histology-genomic integration analysis. PLoS Med 13(2): e1001961
7. Binnewies M, Roberts EW, Kersten K et al (2018) Understanding the tumour immune microenvironment (TIME) for effective therapy. Nat Med 24(5):541–350
8. Fridman WH, Pages F, Sautes-Fridman C, Galon J (2012) The immune contexture in human tumours: impact on clinical outcome. Nat Rev Cance 12(4):298–306
9. Bremnes RM, Busund LT, Kilvaer TL et al (2016) The role of tumour-infiltrating lymphocytes in development, progression, and prognosis of non-small cell lung cancer. J Thorac Oncol 11(6):789–800
10. Galon J, Mlecnik B, Bindea G et al (2014) Towards the introduction of the 'Immunoscore' in the classification of malignant tumours. J Pathol 232(2):199–209
11. Sun R, Limkin EJ, Vakalopoulou M et al (2018) A radiomics approach to assess tumour-infiltrating CD8 cells and response to anti-PD-1 or anti-PD-L1 immunotherapy: an imaging biomarker, retrospective multicohort study. Lancet Oncol 19(9):1180–1191
12. Rizvi NA, Hellmann MD, Snyder A et al (2015) Cancer immunology. Mutational landscape determines sensitivity to PD-1 blockade in non-small cell lung cancer. Science 348(6230):124–128
13. Tumeh PC, Harview CL, Yearley JH et al (2014) PD-1 blockade induces responses by inhibiting adaptive immune resistance. Nature 515(7528):568–571
14. Herbst RS, Soria JC, Kowanetz M et al (2014) Predictive correlates of response to the anti-PD-L1 antibody MPDL3280A in cancer patients. Nature 515(7528):563–567
15. Li B, Cui Y, Diehn M, Li R (2017) Development and validation of an individualized immune prognostic signature in early-stage nonsquamous non-small cell lung cancer. JAMA Oncol 3(11):1529–1537
16. Steele KE, Tan TH, Korn R et al (2018) Measuring multiple parameters of CD8+ tumour-infiltrating lymphocytes in human cancers by image analysis. J Immunother Cancer 6(1):20
17. Yan X, Jiao SC, Zhang GQ, Guan Y, Wang JL (2017) Tumor-associated immune factors are associated with recurrence and metastasis in non-small cell lung cancer. Cancer Gene Ther 24(2):57–63
18. Domagala-Kulawik J, Raniszewska A (2017) How to evaluate the immune status of lung cancer patients before immunotherapy. Breathe 13(4):291–296
19. Grossmann P, Stringfield O, El-Hachem N et al (2017) Defining the biological basis of radiomic phenotypes in lung cancer. Elife 6: e23421
20. Aerts HJ, Velazquez ER, Leijenaar RT et al (2014) Decoding tumour phenotype by noninvasive imaging using a quantitative radiomics approach. Nat Commun 5:4006
21. National Comprehensive Cancer Network (NCCN) (2014) NCCN clinical practice guidelines in oncology: non-small cell lung cancer, V4. 2014. http://www.nccn.org/professionals/physician_gls/pdf/nscl.pdf. Accessed August 15, 2014.
22. Heagerty PJ, Lumley T, Pepe MS (2000) Time-dependent ROC curves for censored survival data and a diagnostic marker. Biometrics 56(2):337–344
23. Fraley C, Raftery AE (2002) Model-based clustering, discriminant analysis, and density estimation. Journal of the American Statistical Association 97(458):611–631
24. El Naqa I, Ten Haken RK (2018) Can radiomics personalise immunotherapy? Lancet Oncol 19(9):1138–1139
25. Maley CC, Koelble K, Natrajan R, Aktipis A, Yuan Y (2015) An ecological measure of immune-cancer colocalization as a prognostic factor for breast cancer. Breast Cancer Res 17(1):131
26. Maley CC, Aktipis A, Graham TA et al (2017) Classifying the evolutionary and ecological features of neoplasms. Nat Rev Cancer 17(10):605–619
27. Pienta KJ, McGregor N, Axelrod R, Axelrod DE (2008) Ecological therapy for cancer: defining tumours using an ecosystem paradigm suggests new opportunities for novel cancer treatments. Transl Oncol 1(4):158–164
28. Merlo LM, Pepper JW, Reid BJ, Maley CC (2016) Cancer as an evolutionary and ecological process. Nat Rev Cancer 6(12):924–935
29. Zwanenburg A, Vallières M, Abdalah MA et al (2020) The image biomarker standardization initiative: standardized quantitative radiomics for high-throughput image-based phenotyping. Radiology 295(2):328–338
30. Tang C, Hobbs B, Amer A et al (2018) Development of an immune-pathology informed radiomics model for non-small cell lung cancer. Sci Rep 8(1):1922
31. Aerts HJ (2016) The Potential of Radiomic-Based Phenotyping in Precision Medicine: a Review. JAMA Oncol 2(12):1636–1642
32. Jiang Y, Wang H, Wu J et al (2020) Noninvasive imaging evaluation of tumour immune microenvironment to predict outcomes in gastric cancer. Ann Oncol 31(6):760–768
33. Rakaee M, Kilvaer TK, Dalen SM et al (2018) Evaluation of tumor-infiltrating lymphocytes using routine H&E slides predicts patient survival in resected non-small cell lung cancer. Hum Pathol 79: 188–198
34. Ogino S, Giannakis M (2018) Immunoscore for (colorectal) cancer precision medicine. Lancet 391(10135):2084–2086
35. Salgado R, Denkert C, Demaria S et al (2015) The evaluation of tumor-infiltrating lymphocytes (TILs) in breast cancer:

recommendations by an International TILs Working Group 2014. Ann Oncol 26(2):259–271
36. Ferris RL, Galon J (2016) Additional support for the introduction of immune cell quantification in colorectal cancer classification. J Natl Cancer Inst 108(8):djw033.
37. Ascierto PA, Capone M, Urba WJ et al (2013) The additional facet of immunoscore: immunoprofiling as a possible predictive tool for cancer treatment. J Transl Med 11:54

Affiliations

Lan He[1] · Zhen-Hui Li[1,2] · Li-Xu Yan[3] · Xin Chen[4] · Sebastian Sanduleanu[5] · Wen-Zhao Zhong[6] · Phillippe Lambin[5,7] · Zhao-Xiang Ye[8] · Ying-Shi Sun[9] · Yu-Lin Liu[10] · Jin-Rong Qu[11] · Lin Wu[12] · Chang-Ling Tu[13] · Madeleine Scrivener[14] · Thierry Pieters[15] · Emmanuel Coche[16] · Qian Yang[10] · Mei Yang[17] · Chang-Hong Liang[1,19] · Yan-Qi Huang[1,18] · Zai-Yi Liu[1,19]

1 Department of Radiology, Guangdong Provincial People's Hospital, Guangdong Academy of Medical Sciences, 106 Zhongshan Er Road, Guangzhou 510080, China

2 Department of Radiology, The Third Affiliated Hospital of Kunming Medical University, Yunnan Cancer Hospital, Yunnan Cancer Center, Kunming, China

3 Department of Pathology, Guangdong Provincial People's Hospital, Guangdong Academy of Medical Sciences, Guangzhou, China

4 Department of Radiology, Guangzhou First People's Hospital, School of Medicine, South China University of Technology, Guangzhou, China

5 The D-lab and the M-lab, Department of Precision Medicine, GROW-School for Oncology, Maastricht University, Maastricht, The Netherlands

6 Guangdong Lung Cancer Institute, Guangdong Provincial People's Hospital, Guangdong Academy of Medical Sciences, Guangzhou, China

7 Department of Radiology and Nuclear Medicine, GROW-School for Oncology and Developmental Biology, Maastricht University Medical Centre+, Maastricht, The Netherlands

8 Department of Radiology, Tianjin Medical University Cancer Institute and Hospital, Tianjin, China

9 Key Laboratory of Carcinogenesis and Translational Research (Ministry of Education/Beijing), Department Radiology, Peking University Cancer Hospital & Institute, Hai Dian District, Beijing, China

10 Department of Radiology, Hubei Cancer Hospital, Tongji Medical College, Huazhong University of Science and Technology, Wuhan, China

11 Department of Radiology, the Affiliated Cancer Hospital of Zhengzhou University & Henan Cancer Hospital, Zhengzhou China

12 Department of Pathology, The Third Affiliated Hospital of Kunming Medical University, Yunnan Cancer Hospital, Yunnan Cancer Center Kunming China

13 Department of Cadres Medical Oncology, The Third Affiliated Hospital of Kunming Medical University, Yunnan Cancer Hospital, Yunnan Cancer Center Kunming China

14 Department of Internal Medicine, Cliniques Universitaires St-Luc, Université Catholique de Louvain, Brussels Belgium

15 Departement of Pneumology, Cliniques Universitaires St-Luc, Université Catholique de Louvain, Brussels Belgium

16 Department of Radiology, Cliniques Universitaires St-Luc, Université Catholique de Louvain, Brussels Belgium

17 Department of Breast Cancer, Cancer Center, Guangdong Provincial People's Hospital, Guangdong Academy of Medical Sciences, Guangzhou China

18 The Second School of Clinical Medicine, Southern Medical University, Guangzhou China

19 Guangdong Provincial Key Laboratory of Artificial Intelligence in Medical Image Analysis and Application, Guangdong Provincial People's Hospital, Guangdong Academy of Medical Sciences, Guangzhou China